SURFACE MODIFICATION OF SILICON AND PDMS SURFACES WITH VAPOR PHASE DEPOSITED ULTRATHIN FLUOROPOLYMER AND FLUOROSILANE FILMS FOR BIOMEDICAL MICRO/NANOELECTROMECHANICAL SYSTEM APPLICATIONS

A Thesis

Presented in Partial Fulfillment of the Requirements for

the Degree Master of Science in the

Graduate School of The Ohio State University

By

Kang Kug Lee, M.S.

*****

The Ohio State University

2005

Master's Examination Committee:

Approved by

Professor Bharat Bhushan, Adviser

Professor Derek Hanford

Adviser

Department of Mechanical Engineering

ABSTRACT

A vapor phase deposition system was designed for the purpose of coating uniform, conformal and ultrathin coatings of fluoropolymer and fluorosilane thin films inside silicon nanochannels. Surface modifications become increasingly important for biomedical micro/nanoelectromechanical system (BioMEMS/NEMS) applications and vapor phase deposition has advantages over liquid phase deposition since the vapor can permeate more efficiently into silicon nanochannels. Vapor phase deposition was used to deposit various ultrathin films, identifying deposition parameters to optimize the process. The films are desirable to control the hydrophobicity of the surface and reduce or prevent undesired protein adsorption or cell interactions, which may cause detrimental effects to the performance of most BioMEMS/NEMS devices. The films were characterized by means of a contact angle analyzer for hydrophobicity and an ellipsometer for film thickness. Atomic force microscopy was used extensively to collect surface images, adhesive and frictional properties of these films, all of which play a very important role in characterizing uniform, conformal and ultra thin films on the surface.

Dedicated to

my lovely LORD, Jesus Christ,

my lovely wife Mi Young Ryu

and my lovely daughter Eun Jong Lee.

ACKNOWLEDGMENTS

I would like to thank first and foremost my LORD, Jesus Christ, for guiding my life. I also want to thank Pastor Keun S. Lee at Korean Church of Columbus for guiding my spiritual aspect. I wish to thank my family members for their unfailing support and encouragement to me throughout my academic career.

I would like to thank my adviser Prof. Bharat Bhushan for giving me an opportunity to work as a graduate research assistant in his state-of-the-art laboratory and for his invaluable guidance. I also thank my co-advisor Prof. Derek Hansford for the opportunity to use cutting-edge facilities at the MicroMD Laboratory and for consenting to be on my Master's Examination Committee.

My special thanks are due to Paul Steffen, manager of the Microfabrication Laboratory and Derek Ditmer, Laboratory Service Coordinator, for their help with the facilities at the MicroMD Laboratory. I also would like to thank Mr. Nick Ferrell for his invaluable technical support. I also want to thank specially the computer systems staff of the Department of Mechanical Engineering, Tom Merrick and Frank Oh, for their help with the computer facilities required to perform my research.

Finally, I thank all my colleagues at Nanotribology Laboratory for Information Storage and MEMS/NEMS (NLIM), especially Dr. Toshi Kasai and Dr. Nikhil Tambe for many helpful discussions in AFM measurements. I also thank Dr. Guohua Wei, Dr.

Zhenhua Tao, Dr. Dharma Tokachichu and Mr. Carmen LaTorre for many helpful discussions. Special thanks to Mr. Zachary Burton for measuring adhesion data using the microtriboapparatus. I also specially thank Caterina Runyon-Spears for her precious help in the lab.

VITA

October 24, 1970……Born – Bukang, Korea

1992……B.S. (Material Science & Engineering)
College of Engineering,
Hanyang University, KOREA

1998-2000…….……..M.S. (Material Science & Engineering)
College of Engineering,
Hanyang University, KOREA

2003-present…….……..Graduate Research Associate,
Mechanical Engineering,
The Ohio State University

PUBLICATIONS

Research Publication

1. Lee, K. K., Bhushan, B., Hansford, D. J. (2005), "Nanotribological Characterization of Fluoropolymer Thin Films for BioMEMS/NEMS Applications," *J. Vac. Sci. & Technol. A* **23(4)**.
2. Lee, K. K., Cha, N. G., Kim, J. S., Park, J. G., Shin, H. J. (2000), "Chemical, Optical and Tribological Characterization of Perfluoropolymer Films as an Anti-stiction Layer in Micro-mirror Arrays," *Thin Solid Films*, **377-378**, pp. 727-732.
3. Park, J. G., Kwon, M. J., Lee, K. K., Kim, Y. K., Shin, H. J. (1998), " The Vapor Phase Deposition of Fluorocarbon Films for the Prevention of In-use Stiction in Micromirror", *Japanese Journal of Applied Physics*, **37**, No 12B, pp. 7058 – 7063.

FIELDS OF STUDY

Major Field: Mechanical Engineering

TABLE OF CONTENTS

LIST OF TABLE

LIST OF FIGURES

CHAPTER 1

INTRODUCTION

BioMEMS/NEMS have the potential to revolutionize medical diagnostics and biological experimental processes (Kricka, 2001; Bhushan, 2004). BioMEMS/NEMS devices have become the logical approach to satisfy the requirements for cost efficient medical devices that are capable of analyzing, filtering, and manipulating minute volumes. The utilization of the microfabrication technology has produced such MEMS/NEMS -based instrumentation as flow cytometers, biological assays, and nano-filters (Desai et al., 2000a; Hansford et al., 2001). Several applications have been proposed based on silicon, glass, or polymer nanochannels (conduits with one minimum dimension <100nm), including cell immunoisolation chambers, protecting biosensors from fouling, DNA separation devices, and entropic barriers for molecular separations (Hansford et al., 2001). For gas-based separations based on nanochannels, having hydrophobic surfaces provides several advantages, including low fouling and higher gas transport rates.

One application of nanochannel membranes is the microencapsulation of cells or other biological tissues for the transplantation of cells for biological function replacement. A schematic diagram of the microfabricated biocapsule is shown in Fig. 1.1(a), showing the exclusion of immune molecules (with sizes of ≥ 15 nm) while allowing the passage of insulin and nutrients (sizes of ≤ 6 nm). As shown in Fig. 1.1(b),

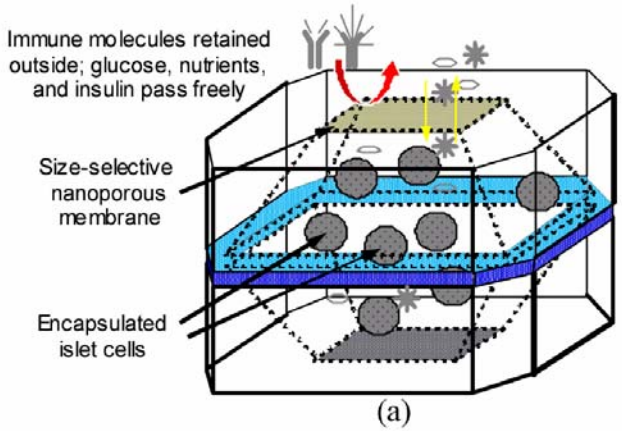

(a)

(b)

Figure 1.1: (a) Schematic diagram of basic microfabricated immunoisolation biocapsule concept, (b) One-half of immunoisolation biocapsule (Hansford et al., 2001).

the biocapsule consists of two separate microfabricated membranes bonded together with the desired cells contained within the cavities. In order to fabricate a membrane with highly defined channels, it was necessary to develop a robust protocol that could use standard microfabrication processes (Desai et al., 1999, 2000b; Hansford et al., 2001).

The fabrication of nanochannels can be accomplished through several routes. Direct writing of nanostructures using e-beam lithography provides high fidelity features, but requires serial processing and is thus a slow process. The use of a sacrificial layer allows the direct control of nanochannel dimensions so long as there exists a method for removing the sacrificial layer with absolute selectivity to the structural layers. A materials system with such selectivity is the silicon/ silicon oxide system used widely in the microfabrication of MEMS devices. The use of sidewall deposition of the sacrificial layer and subsequent etching allows for the fabrication of high density nanochannels for biomedical applications (Desai et al., 2000a; Hansford et al., 2001). Fig. 1.2 shows a schematic representation of the fabrication protocol, called the D1 design (Hansford et al., 2001). As with all the membrane protocols, the first step in the fabrication was the etching of the support ridge structure into the bulk silicon substrate. A low stress silicon nitride (LSN or nitride), which functioned as an etch stop layer, was then deposited using low pressure chemical vapor deposition (LPCVD). The base structural polysilicon layer (base layer) was deposited on top of the etch stop layer. Because the etch stop layer did not fill the machined ridges, the structural layer was deposited down into the support ridge, which remained after the membrane was released and the etch stop layer was removed. The etching of holes in the base layer was

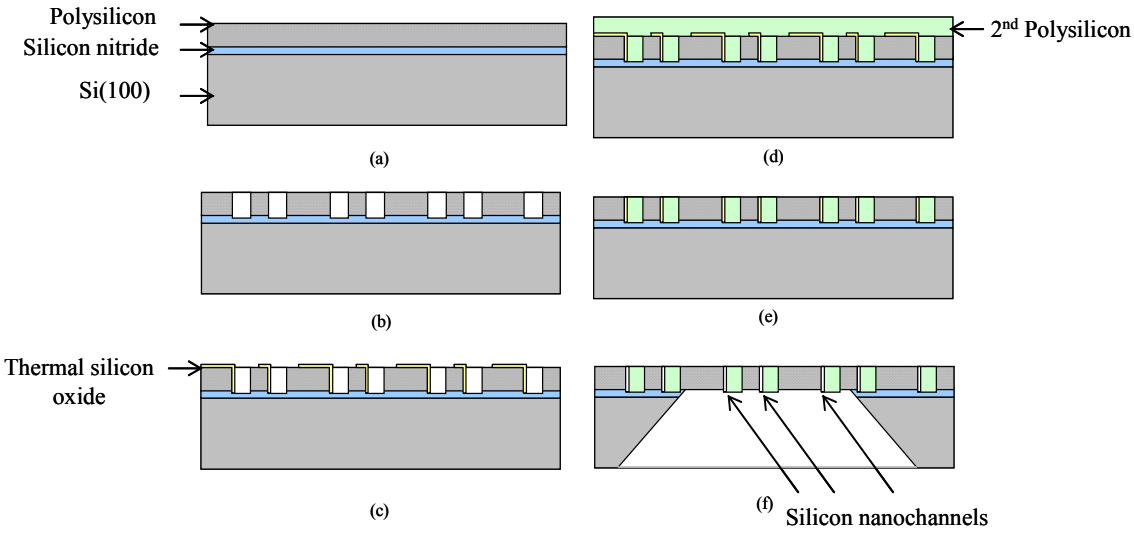

Figure 1.2: D1 design process: (a) growth of buried nitride layer; base polysilicon deposition; (b) hole definition in base; (c) growth of thin sacrificial oxide and patterning of anchor points; (d) deposition of plug polysilicon; (e) planarization of plug layer; (f) deposition and patterning of protective nitride layer, and through etch; final release of structure in HF (Hansford et al., 2001).

what defined the shape of the pores. In this step, it was important to make sure the etching went completely through the base layer, so an overetch was used. It is useful to note that the buried nitride etch stop acted as an etch stop for the plasma etching of a silicon base layer. After the pore holes were defined and etched through the base layer, the pore sacrificial oxide was grown on the base layer. The basic requirement of the sacrificial layer is the ability to control the thickness with high precision across the entire wafer. Thermal oxidation of polysilicon allowed the control of the sacrificial layer thickness of less than 5% across the entire wafer. Anchor points are defined in the sacrificial oxide layer to mechanically connect the base layer with the plug layer (necessary to maintain the pore spacing between layers). This was accomplished by using the same mask shifted from the pore holes by 1 μm diagonally. This produced anchors in one or two corners of each pore hole, which provided the desired connection between the structural layers while opening as much pore area as possible. After the anchor points were etched through the sacrificial oxide, the plug polysilicon layer was deposited (using LPCVD) to fill in the holes. To open the pores at the surface, the plug layer was planarized using chemical mechanical polishing (CMP) down to the base layer, leaving the final structure with the plug layer only in the pore hole openings. As the membrane was ready for release, a protective nitride layer was deposited on the wafer (completely covering both sides of the wafer). The backside etch windows were etched in the protective layer, exposing the silicon wafer in the desired areas, and the wafer was placed in a KOH bath to etch. After the silicon wafer was completely removed up to the membrane (as evidenced by the smooth buried etch stop layer), the protective, sacrificial, and etch stop layers were removed by etching in concentrated HF

(Hansford et al., 2001). Fig. 1.3 shows micrographs for a 25 nm channel and a 50 nm channel in silicon membranes fabricated using such a technique.

Micro/nanofluidic systems provide a powerful platform for electrophoretic separations for a variety of biochemical and chemical analysis (Kricka, 2001; Mitchell, 2001). In micro/nanofluidics, small volumes of solvent, sample, and reagents are moved through micro/nanochannels. Examples of bioassays and biological procedures include DNA sequencing, electrophoresis, DNA separation, enzymatic assays, immunoassays, cell counting, cell sorting, and cell culture. Electrophoresis is a versatile analytical technique which is successfully used for the separation of small ions, neutral molecules, and large biomolecules. It is being utilized in widely different fields, such as analytical chemistry, clinical chemistry, organic chemistry, and pharamaceutical industry (McDonald and Whitesides, 2002; Auroux et al., 2002). Miniaturizations of bioassays offer many advantages, including high-throughput screening for solvents, reagents, and cells, short reaction times, portability, low cost, low consumption of power, versatility in design, and potential for parallel operation and for integration with other miniaturized devices. Immunoassays combine the principles of chemistry and immunology enabling scientific tests, e.g. enzyme immunoassays and immunoblotting for a specific and sensitive detection of the analytes of interest. The basic principle of these assays is the specificity of the antibody-antigen reaction. Though being very specific and sensitive immunoassays are easy to perform which has contributed to the widespread use and tremendous success (Auroux et al., 2002). For gas-based separations based on nanochannels, having hydrophobic surfaces provides several advantages, including low

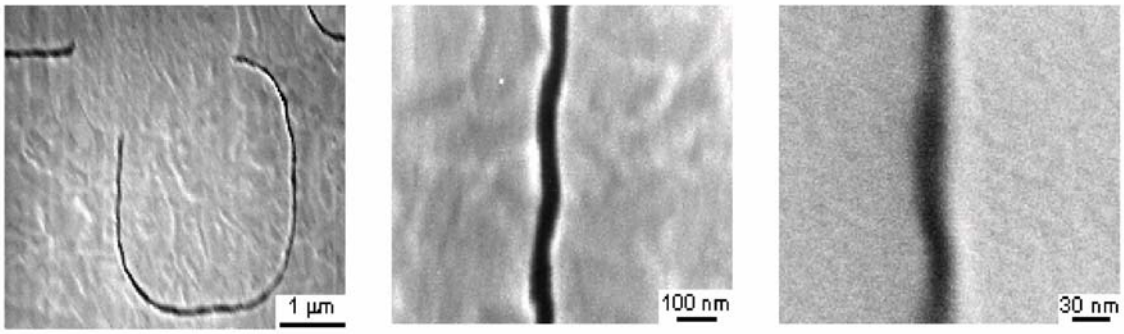

Figure 1.3: Scanning electron micrographs of silicon nanochannels showing: (a) a single 50 nm channel; (b) high magnification image channel; and (c) high magnification image of 25 nm channel (Hansford et al., 2001).

fouling and higher gas transport rates. Micrograph of an interdigitated micro/nanofluidic array is shown in Fig. 1.4(a), showing nanochannels for separation process. Fig. 1.4(b) shows an SEM exploded view of silicon nanochannels.

Surface chemistry is of great importance in micro/nanofluidic devices especially in highly miniaturized and integrated systems due to the high surface area-to-volume ratio. The surface modification (Wang and Ferrari, 2000; Popat et al., 2002; Cox et al., 2002; Liu and Bhushan, 2003a) of interior surfaces of nanochannels presents many problems. Transport of reactive species, self-limiting reactions, uniform distribution of reactants, and complete coverage of surfaces are several limitations of most techniques, including liquid phase deposition. The use of low pressure vapor phase deposition allows many of these limitations to be overcome (Liu and Bhushan, 2002; Lee et al., 2005). Surface modifications using vapor phase deposition become increasingly important for some biomedical nanodevices and have advantages over liquid phase deposition since the vapor phase can permeate more efficiently into nanochannels.

Polydimethylsiloxane (PDMS)-based elastomers have been used in a wide range of biomedical applications in the past three decades, as a result of their physiological inertness, good blood compatibility, low toxicity, good thermal and oxidative stability, low modulus and antiadhesive properties. Medical devices based on PDMS include blood pumps, cardiac pacemaker leads, mammary prostheses, drainage implants in glaucoma, artificial skins, drug-delivery systems and denture liners (Sia and Whitesides, 2003).

The objective of this study was first to construct a vapor phase deposition system capable of accommodating 100 mm (4 inch) silicon wafers or an array of silicon chips with microfabricated nanochannels. Films of two fluoropolymers (CYTOP^{TM} and Fluorinert^{TM}) and four fluorosilanes (PFOTCS, PFODCS, PFDTES, and PFPTES) were deposited onto silicon and PDMS surfaces to study the deposition parameters and identify an optimized deposition protocol. Modified surfaces were characterized using several techniques - static contact angle, ellipsometer and atomic force microscopy (AFM) (Wallace et al., 1999; Liu and Bhushan, 2002, 2003a; Popat et al., 2003; Bhushan, 2004). We will particularly focus on the vapor deposition conditions and nanotribological behavior of the hydrophobic fluoropolymer thin films. The surface images, adhesive and frictional properties of these films were examined using AFM.

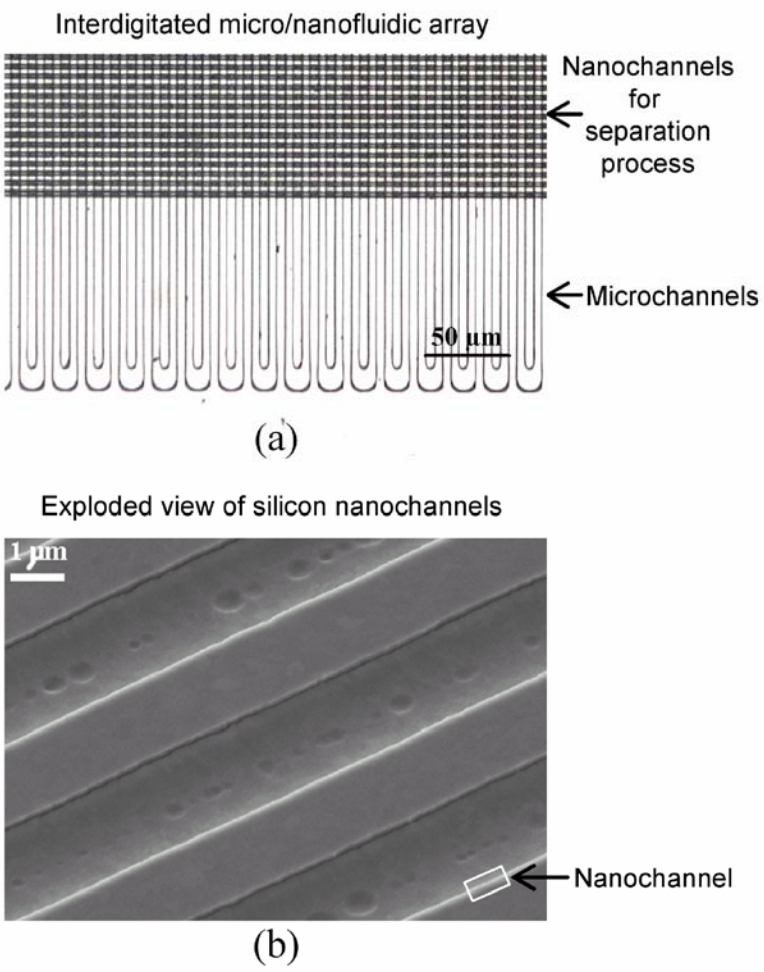

Figure 1.4: Micrographs of silicon nanochannels prior to etching the microfluidic channels: (a) optical image of interdigitated micro/nanofluidic device, with the microfluidics connected by 5 micron long nanochannels (20 nm wide channels), (b) SEM exploded view of silicon nanochannels (personal communication with Prof. Hansford, 2005).

CHAPTER 2

EXPERIMENTAL DETAILS

2.1. Materials and experimental procedures

Test grade silicon wafers (p-type, <100> orientation) and PDMS (Silastic T2, Dow Corning) were prepared as substrates in this study. Two kinds of fluoropolymer chemicals, CYTOP^{TM} (CTL-107M, solute and CT-SOLV100, solvent, Asahi Glass, Charlotte, USA) and Fluorinert^{TM} (SJ040715C, FC722, solute and FC72, solvent, 3M, Seoul, Korea) and four kinds of fluorosilane precursors, PFOTCS, PFODCS, PFDTES, and PFPTES (ABCR GmbH & Co. KG, Karlsruhe, Germany) were used for the vapor phase deposition. Fig. 2.1 and Fig. 2.2 schematically show the chemical structures of the chemicals deposited on surfaces in this study. Their typical properties are summarized in Table 2.1.

In the case of silicon substrate, the silanes react with native oxide formed on the silicon substrate to form covalent bondings. The trifunctional silanization reaction occurs for silanes, a head group of the vapor silane, with three active groups attached to the silicon atoms in the case of the PFOTCS, PFDTES, and PFPTES films. After the silanes react with hydroxyl groups on the surface, strong covalent bondings are formed on the silicon surface. The monofunctional silanization reaction occurs for silanes with one active group in the case of the PFODCS film.

The silicon wafers were first cut into 15 mm × 15 mm rectangular shapes for the experiment. All wafers were cleaned by immersion in Piranha solution (a mixture of 3:1 v/v 98% sulfuric acid: 30% hydrogen peroxide) at 90 °C for 30 minutes followed by a triple rinse in deionized water. The wafers were then immersed in 49% HF solution for 10 minutes to remove the native oxide followed by another triple rinse with deionized water and dried with high-pressure high-purity nitrogen gas as depicted in Fig. 2.3. Another surface treatment for silicon wafers was cleaning in Piranha solution (a mixture of 3:1 v/v 98% sulfuric acid: 30% hydrogen peroxide) at 90 °C for 30 minutes followed by a triple rinse in deionized water. Oxygen plasma treatment was used to clean the PDMS surfaces and silicon wafers. The wet cleaned silicon wafers, the Piranha cleaned silicon wafers and PDMS were placed in a vapor phase deposition system (Lee et al., 2005) for the film deposition. Nitrogen from the gas cylinder was passed through a glass tube connected with glass source cup, passed through the chamber and flowed over the silicon substrates inside the chamber. Chemicals were vaporized in the glass source cup using a heating tape. The chemical vapors were picked up by the carrier nitrogen and deposited on the silicon surface to form thin polymer films inside the vacuum chamber.

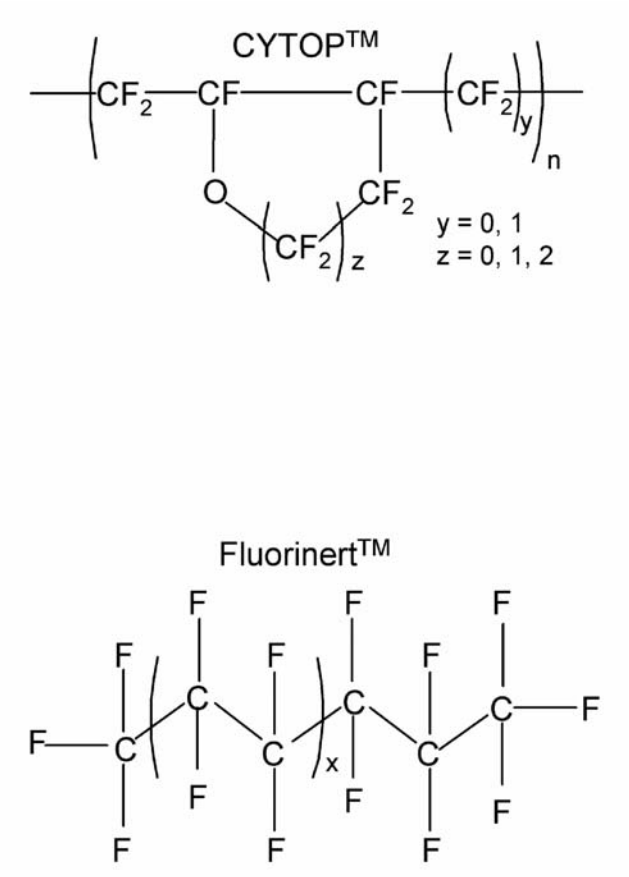

Figure 2.1: Chemical structures of two fluoropolymers, CYTOP™ and Fluorinert™.

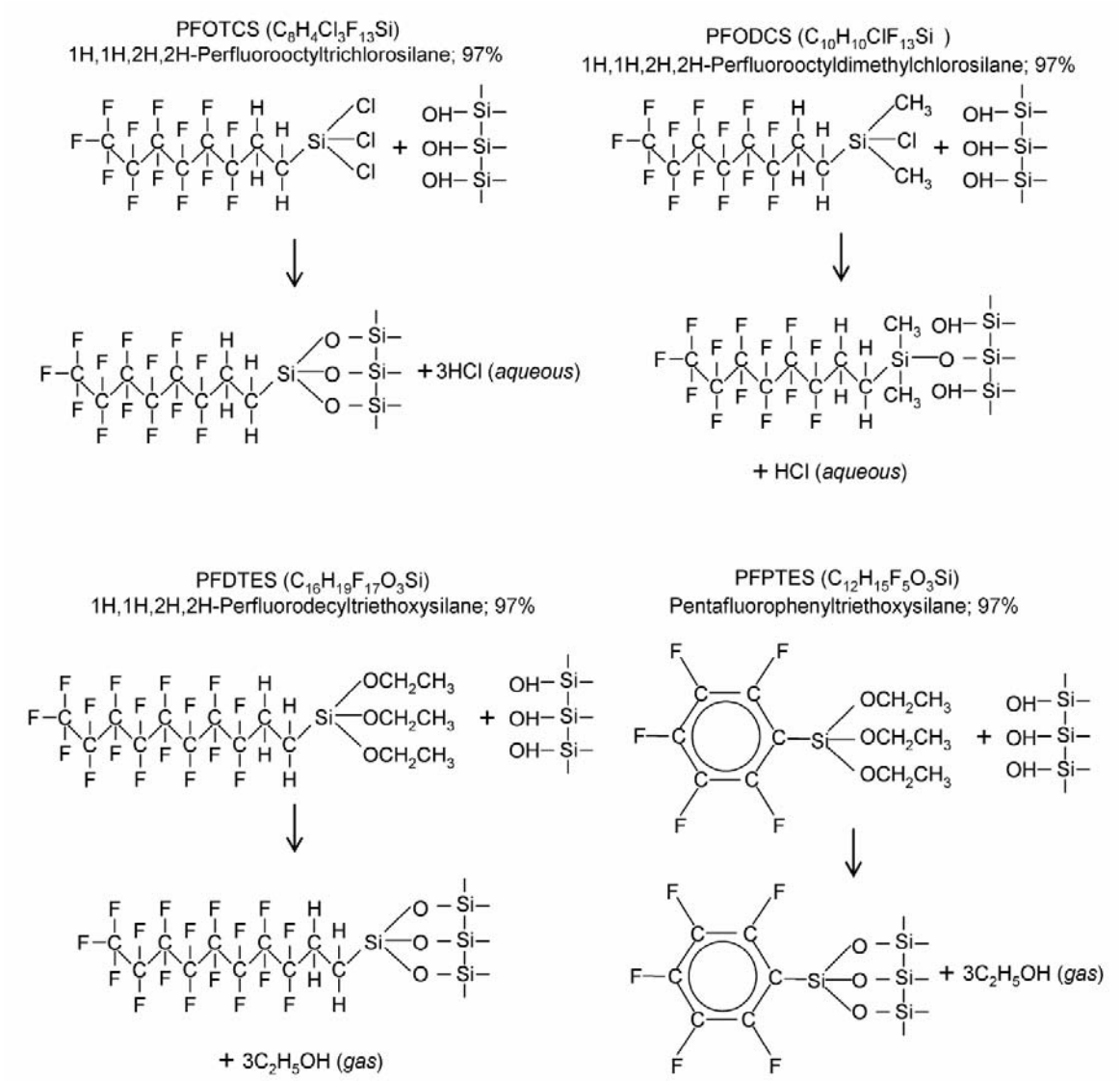

Figure 2.2: Chemical structures of fluorosilane films deposited on Piranha cleaned silicon substrates.

Properties	CYTOP™	Fluorinert™	PFOTCS	PFODCS	PFDTES	PFPTES
Molecular weight	-	340	481.54	440.72	610.38	330.33
Density (g/cm^3)	2.03	1.68	1.638	1.473	1.407	1.24
Boiling point (^oC)	97-102	56	84-85	189-191	103-106	130
Vapor pressure (Torr)	42-46	232	-	-	-	-
Glass transition temperature (^oC)	108	-	-	-	-	-
Surface tension (dynes/cm)	19	12	-	-	-	-
Water adsorption	<0.01 %	-	-	-	-	-
Durometer hardness	HDD78	-	-	-	-	-
Thermal conductivity (W/m.K)	0.11	0.057	-	-	-	-
Coefficent of expansion (/ ^oC)	7.4×10^{-5}	1.6×10^{-3}	-	-	-	-

Table 2.1: Properties of two fluoropolymers, CYTOP™, Fluorinert™, and four fluorosilanes, PFOTCS, PFODCS, PFDTES and PFPTES.

2.2. Vapor phase deposition system

A schematic diagram of the apparatus for vapor phase deposition is shown in Fig. 2.4. The system consists mainly of three parts: a vacuum chamber, a glass source cup and a glass tube and a nitrogen gas flow system. The vapor phase deposition process was carried out in a vacuum chamber (VWR model 1400E, 110V, 50/60Hz, 550W). The valves and fittings from Swagelok (No. SS-42S4, SS-400-3 and SS-400-9) were used as connectors between Teflon tubings. All Teflon tubings for the system were from Fisher (No. 14-176-179, 890FEP). The glass tube and the glass source cup were designed for this system with input and output port valve plugs and O-rings for sealing. The glass tube and the glass source cup were connected using a clip and O-ring for sealing. These features provide a convenient way to fill chemicals by separating the glass tube from the glass source cup. A heating tape used for heating the glass source cup, glass tube and Teflon line was a FluidX model (No. BHBSAT101002, Salt Lake City). The chemicals were put into the glass source cup, which was maintained at constant temperature during processing by a heating tape. The final major component in this system is the nitrogen carrier gas system. Ultra-high-purity nitrogen gas was dispensed from the gas cylinder using a pressure regulator before it was delivered to the glass tube and source cup. The nitrogen gas could either be introduced into the by-pass line or the direct flow line over the glass source cup. The by-pass line was used before and after the deposition process to purge the chamber, and the direct flow line was used during the deposition processes. After the samples were loaded, nitrogen gas was used to purge the chamber of moisture for about 5 minutes. Following this purge step, the deposition process for the CYTOP^{TM} and Fluorinert^{TM} consisted of a vapor injection

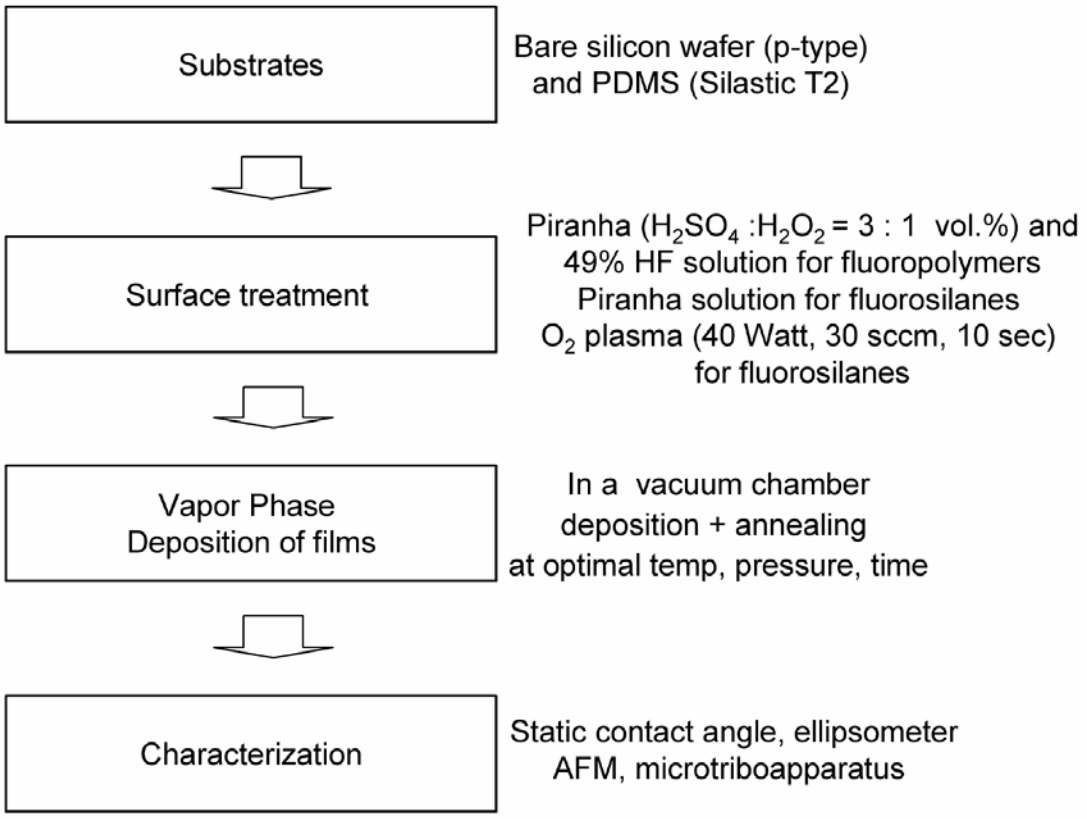

Figure 2.3: Flow chart of procedure for vapor phase deposition.

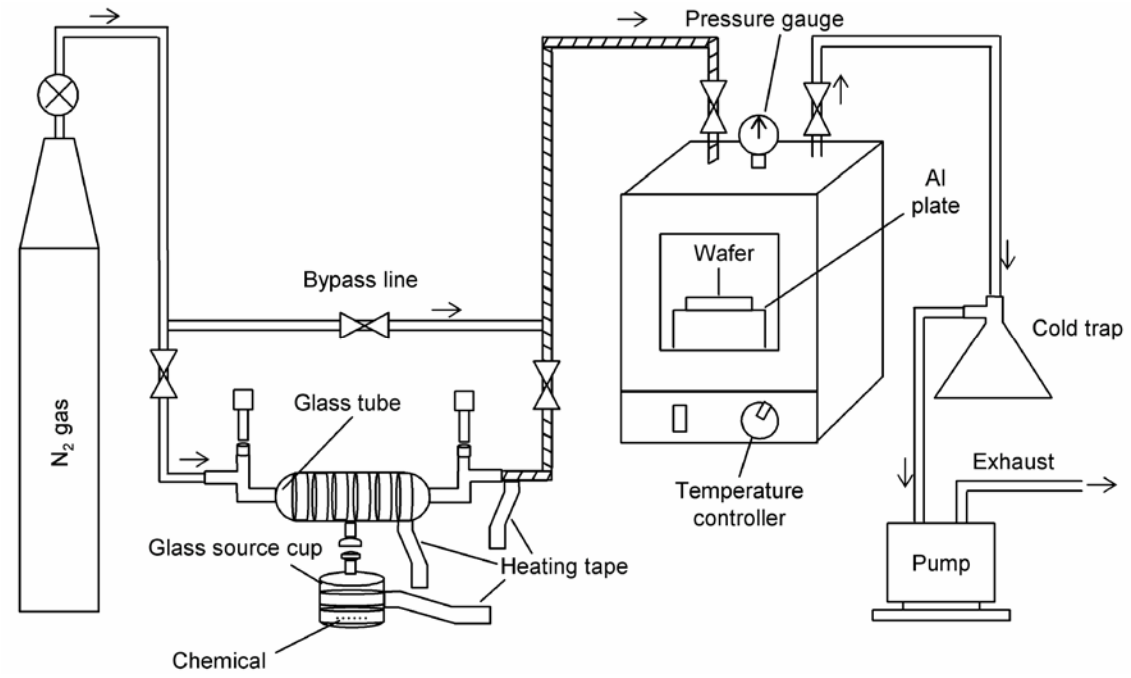

Figure 2.4: Schematic diagram of the apparatus for vapor phase deposition of polymer thin films.

into the chamber until a pressure of 200 Torr was achieved, at which point the vacuum line and carrier gas line were closed. For the fluorosilane deposition, a steady-state chamber pressure of 200 Torr was achieved by flow control of the carrier nitrogen gas and the vacuum line. The carrier gas helps to remove excess, unreacted chemicals. The deposition process was followed by an annealing step for 20 minutes. Once the deposition process was completed, the inlet/outlet valves were closed to isolate the glass tube and pump down the chamber. After the deposition was completed, typically 50 minutes, the by-pass carrier gas line was opened, introducing pure nitrogen gas into the vacuum chamber to complete the removal of by-products and non-reacted chemicals. Finally, the samples were removed from the vacuum chamber and transferred into a vacuum desiccator until characterization.

2.3. Analytical methods

In this study, static contact angles with high purity deionized water (18.2 MΩcm) were measured in air by a sessile-drop method using a contact angle goniometer (Model 100, Rame-Hart Inc., Mountain Lakes, NJ, USA) in order to determine the hydrophobicity of the modified surfaces. 5 μL of deionized water was applied on the sample surfaces using a micropipette. Three contact angle measurements were taken on each sample. This was repeated for a total of two samples. Reported measurements are averages of the measurements on two samples.

The thickness of the polymer film was measured on a Gaertner L116SF ellipsometer, which was equipped with a He–Ne laser (632.8 nm) set at an incident angle of 70° to maximize the sensitivity in the range close to the Brewster angle of the

films. The refractive indices of 1.34 and 1.36 were assumed for CYTOP^{TM} and Fluorinert^{TM} thin films, respectively. A value of 1.34 was estimated for four fluorosilane thin films. Over ten replicate measurements were carried out for each specimen. The effective thickness is the difference between the thickness of modified and unmodified silicon.

The nanotribological behavior of the polymer thin films was characterized on a commercial AFM system (Digital Instrument, Santa Barbara, CA) (Bhushan, 2004). Square pyramidal Si_3N_4 tips with a nominal 30–50 nm radius mounted on goldcoated triangular Si_3N_4 cantilevers with spring constants of 0.58 N/m were used. By measuring the friction force as a function of normal load, an average value of the coefficient of friction was obtained. To obtain the adhesive force between the AFM tip and the film surface, the force–distance curve was recorded and the pull-off force reckoned as the adhesive force. The adhesive forces were also calculated from the horizontal intercept of friction versus normal load curves at a zero value of friction force. The AFM images were obtained under ambient conditions and all the scans were one micron in size.

A microtriboapparatus (Tetra Inc., Ilmenau, Germany) was used to measure the adhesive force between the silicon and the film surfaces (Liu and Bhushan, 2003b). A single crystal Si (100) ball (1 mm in diameter, 5×10^{17} atoms/cm^3 boron doped) was mounted on a stainless steel cantilever. It has a native oxide layer on their surfaces. This apparatus has the following advantages: it can deliver velocity higher than that in AFM; a large radius or flat specimen can be used to reduce the contact stress; and MEMS/NEMS components can be directly mounted on this machine for tribological tests.

CHAPTER 3

RESULTS AND DISCUSSION

3.1 Fluoropolymer films

3.1.1 Static contact angle, thickness, and roughness variation of vapor phase deposited films

The static contact angle, thickness and roughness variation of two fluoropolymer films were plotted as a function of pressure, processing time and temperature in Fig. 3.1. The contact angle analysis is a simple, but a very powerful method for measuring the changes of surfaces at the monolayer level. In order to optimize the vapor phase deposition conditions, the static contact angles were measured after the film deposition as a function of pressure, processing time and temperature. The deposited film with the highest contact angles and lowest standard deviations determined the optimum process conditions. Pre-process conditions were designed before optimizing process conditions. A two-step vapor phase deposition process was applied in this study; first, samples were left in a vacuum chamber at its base pressure, and then, the samples were annealed at a higher pressure induced by nitrogen gas filling in the same chamber and at the same temperature. The first deposition process was carried out for 20 min and the second annealing process was also performed for 20 min to find the optimum temperature, 140^{o}C, as shown in Fig. 3.1. At 140^{o}C, the optimum pressure 200 Torr was also determined by the measurements of contact angles as shown. The length of processing

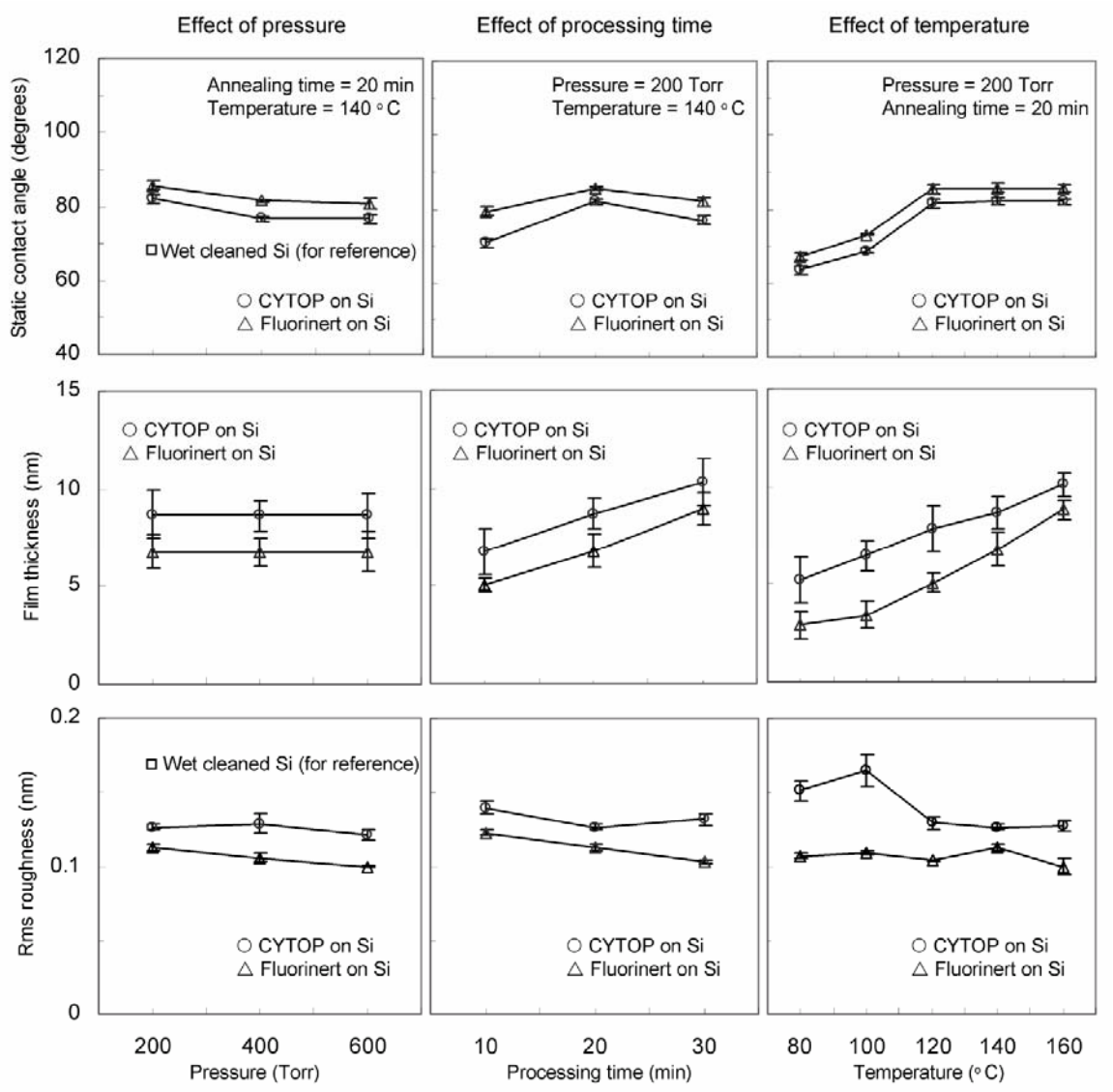

Figure 3.1: Static contact angle, film thickness and Rms roughness measurement as a function of pressure, annealing time and temperature.

time 20 min was also determined using contact angle measurement under the temperature and pressure obtained from the above. The optimized vapor deposited surfaces showed an increase in contact angle (contact angle ~85°) as compared to the wet cleaned silicon surface (contact angle ~68°). From the observations above, it can be concluded that the surface modified by the fluoropolymer films has a higher water contact angle than the silicon surfaces. The surface wettability was considerably modified to hydrophobic by the vapor phase deposition.

As expected, the results showed the film thickness of CYTOP™ and Fluorinert™ on silicon was increased as a function of processing time and temperature. As can be seen in Fig. 3.1, the decrease in rms roughness for the vapor phase deposited films was found as compared to the wet cleaned silicon substrate, which suggests that the coatings decrease the surface roughness. The native oxide on silicon is chemically more heterogeneous, and the capillary formation may not be uniform during scanning. This could affect AFM topography measurements because of heterogeneous adhesive forces due to the capillary effect. The capillary formation may be more uniform for the vapor phase deposited samples, explaining the reduced rms roughness for the samples. The rms roughness values of the CYTOP™ were decreased as a function of temperature, while that of Fluorinert™ remained relatively constant with temperature.

3.1.2 Frictional properties of vapor phase deposited films

Figure 3.2(a) shows gray-scale images of surface height and friction force captured simultaneously of wet cleaned silicon, CYTOP™ and Fluorinert™ on silicon over a region of 1 μm 3 1 μm by contact mode AFM. The topography of silicon surface

appears to be heterogeneous. The roughness values decreased with film deposition. The friction force maps in Fig. 3.2(a) clearly show the reduction in friction force for the CYTOP™ and Fluorinert™ on silicon as more uniform contrast, compared with the wet cleaned silicon. For all the surfaces, a good correlation between the surface height and the corresponding friction force images was observed.

To investigate the frictional properties of the vapor phase deposited films on silicon, the friction force versus normal load curves were measured by making friction measurements at increasing normal loads. The representative results of wet cleaned silicon, CYTOP™ and Fluorinert™ on silicon are shown in Fig. 3.2(b). An approximately linear response of all the three samples is observed in the load range. The friction force of the CYTOP™ and Fluorinert™ films on silicon is consistently smaller than that for wet cleaned silicon. The non-zero value of the friction signal at zero external loads is due to the adhesive forces. It is well known that the following relationship exists between the friction force F and external normal load W (Bhushan, 1999, 2002; Bhushan and Liu, 2001, 2002; Liu and Bhushan, 2003b)

$$F = \mu(W + W_a), \tag{1}$$

where μ is the coefficient of friction and Wa is the adhesive force. Based on this equation and the data in Fig. 3.2(b), we can calculate the μ and Wa values. Since the coefficient of friction was affected by the vapor phase deposition, the vapor phase deposited films on silicon showed an improvement in coefficient of friction as compared to the silicon substrate. The coefficients of friction of wet cleaned silicon, CYTOP™ and Fluorinert™ are 0.06, 0.055 and 0.056, respectively. Based on Eq. (1), the adhesive force values are obtained from the horizontal intercepts of the friction

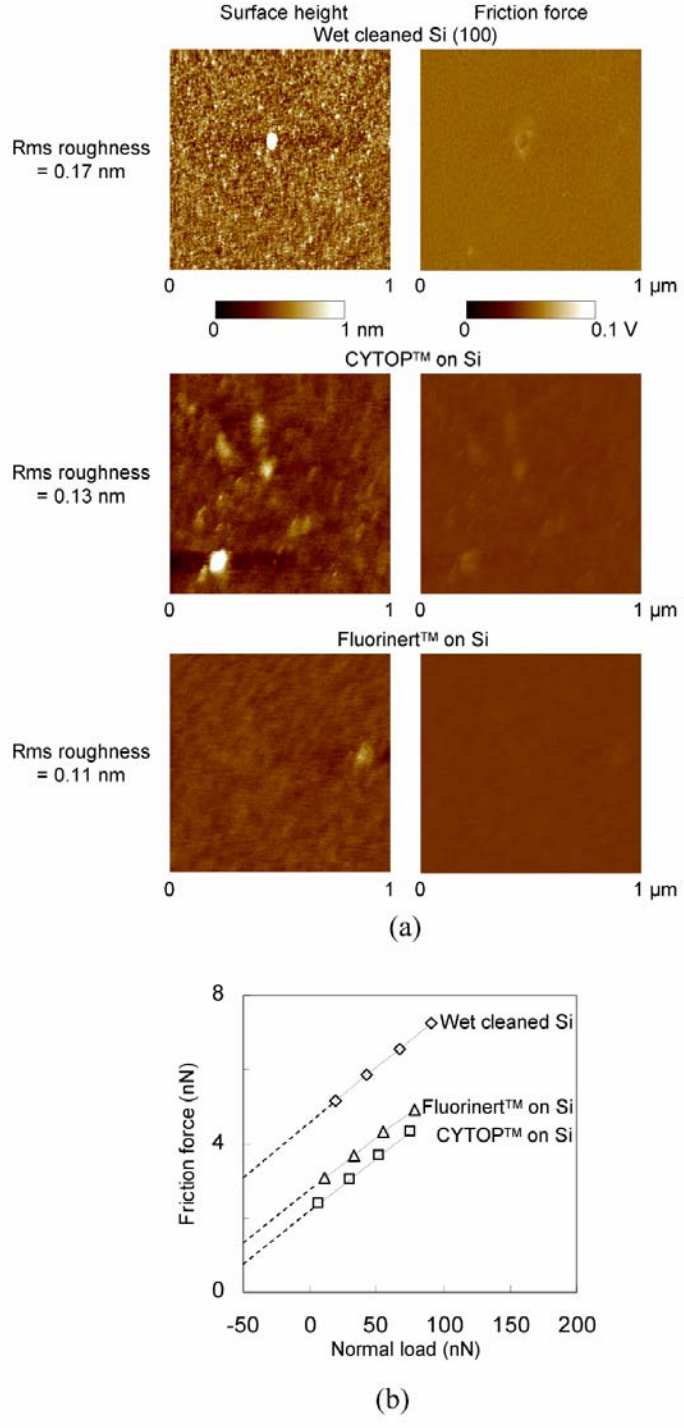

Figure 3.2: (a) Surface height and friction force maps for wet cleaned Si, CYTOP^{TM} on Si, and Fluorinert^{TM} on Si, (b) Friction force verses normal load.

force versus normal load curves at a zero value of friction force. The average values and standard deviation of the static contact angles, adhesive forces and coefficients of friction measured by contact mode AFM (Bhushan, 1999, 2002; Bhushan and Liu, 2001, 2002; Liu and Bhushan, 2003b) are presented in Fig. 3.3. Corresponding surface height and friction maps are also shown in Fig 3.2(a). It shows that vapor deposited films can reduce the adhesive and frictional forces of silicon. In particular, CYTOP™ and Fluorinert™ exhibits lower adhesive and frictional forces than the silicon substrate. It means that these fluoropolymer films can be used as effective lubricants or barriers for micro/nanodevices fabricated from silicon. In the third diagram of Fig. 3.3, adhesive force values of wet cleaned silicon, CYTOP™ and Fluorinert™ are 78, 50, and 55 nN, respectively. The adhesive forces of these samples were also measured by force calibration method. In this technique, the tip is brought into contact with the sample and the maximum force, needed to pull the tip and sample apart, is measured (Bhushan, 1999, 2002; Bhushan and Liu, 2001, 2002; Liu and Bhushan, 2003b). The adhesive forces of wet cleaned silicon, CYTOP™ and Fluorinert™ films were also measured by the microtriboapparatus (Liu and Bhushan, 2003a) and the measured adhesive forces were summarized in the last diagram of Fig. 3.3. The adhesive force values are 670, 622, and 483, respectively. It shows that the presence of fluoropolymer films reduces the adhesive force of silicon, whereas Fluorinert™ film has the lowest adhesive force. Differences of the data between the different techniques are due to differences in the tip material, shape and scale of the microtriboapparatus compared to the AFM. In the nanochannel system, it is critical to obtain hydrophobic, uniform and conformal ultrathin films deposited inside the nanochannels. The hydrophobic polymer films have

lower adhesive and frictional forces than the silicon substrate in this paper. Characterization of the static contact angle, frictional forces, and adhesion forces of the vapor deposited films demonstrates the usefulness of this process for these applications.

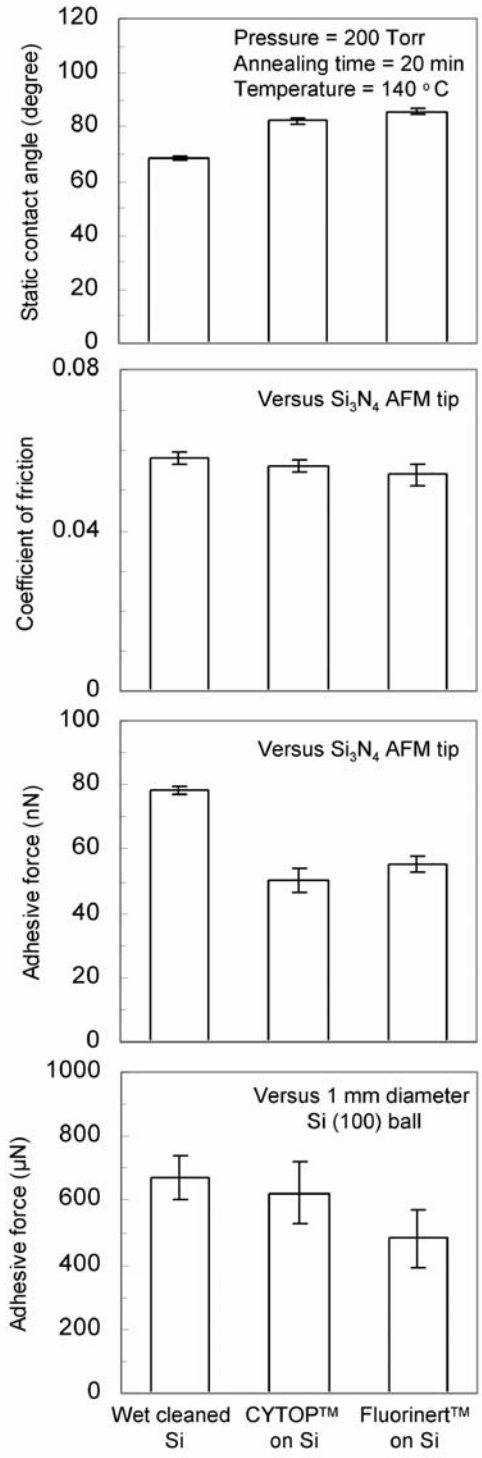

Figure 3.3: A summary of static contact angle, coefficient of friction and adhesive forces for wet cleaned Si, CYTOP™ on Si, and Fluorinert™ on Si.

3.2 Fluorosilane SAM films

Fig. 3.4(a) shows static contact angle (SCA) variations of the substrates. The SCA value of the untreated PDMS is 105° which is hydrophobic. The surface of the PDMS is $–CH_3$ termination group. The SCA values of oxygen plasma treated PDMS, Piranha cleaned silicon, and oxygen plasma treated silicon was low compared with those of untreated PDMS and HF cleaned silicon. It shows that they have the same surface chemistry and –OH termination group, which is hydrophilic. The SCA value of HF cleaned silicon is 68° because the surface has –H termination group, which makes it slightly hydrophobic. As the films were deposited on the surfaces, the SCA values of the films increased as shown in Fig. 3.4(b). This shows the dependency on the initial surface treatment processes of the films. The highest SCA value was obtained in the PFDTES films. The SCA value of the oxygen plasma treated PDMS is slightly higher than those of Piranha cleaned silicon and oxygen plasma treated silicon. The SCA value of the films on Piranha cleaned silicon is almost the same as that of the films on oxygen plasma treated silicon since they have a same surface termination group. The adhesive forces (Fig. 3.4(c)) of the films using force calibration method shows that the presence of fluorosilane films reduces the adhesive force of substrates, whereas PFOTCS film has the lowest adhesive force. Characterization of the static contact angles and adhesion forces of the films demonstrates the usefulness of vapor phase deposition process.

The SCA and thickness variation of the four kinds of fluorosilane films were plotted as a function of temperature, pressure and deposition time in Fig. 3.5. In order to optimize the deposition conditions, the SCA and the film thickness were used as references after the film deposition. For ethoxy silanes, the deposition process was 20

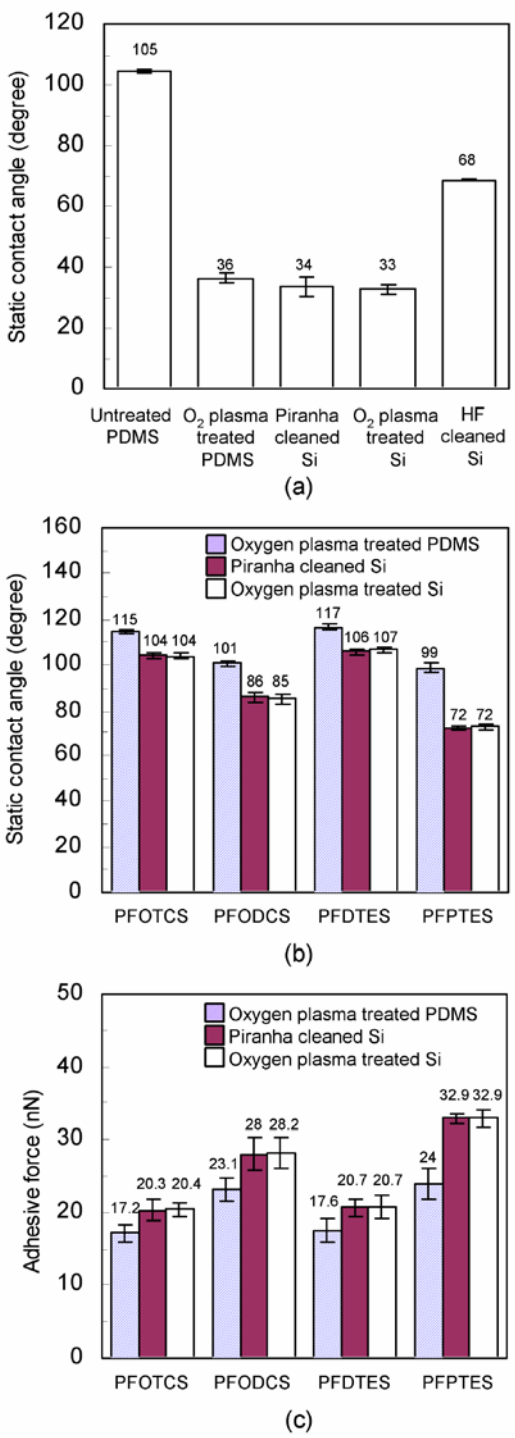

Figure 3.4: A summary of static contact angle variation of (a) different surface treated substrates, (b) four different kinds of fluorosilanes, and (c) adhesive forces of four different kinds of fluorosilanes.

min and the annealing process was also 20 min to find the optimum temperature, 100^{o}C and 160^{o}C for PFDTES and PFPTES, respectively. For chloro silanes, a 5 min deposition was used to find the optimum temperature, 40^{o}C and 80^{o}C for PFOTCS and PFODCS, respectively. The optimized PFDTES film on silicon surface showed a large increase in SCA value (~106°) as compared to the Piranha cleaned silicon surface (~34°). The optimum pressure 200 Torr was also determined based on the SCA values. However, the optimum pressure of the PFDTES film was 400 Torr based on the film thickness measurements. From the above observations, it can be concluded that the surface modified by the fluorosilane films has a higher water contact angle than the silicon surfaces. The surface wettability could be considerably modified to hydrophobic by the vapor phase deposition. The film thickness of the four films on silicon was not affected by temperature, pressure, and deposition time because the film was coated as a monolayer. However, there was a large decrease of film thickness as a function of pressure for the PFDTES film. This may be because the crosslinking between silanes might be produced in the lower pressure.

The rms roughness value of the Piranha cleaned silicon was measured as 0.16 nm. The rms roughness values of the PFOTCS, PFODCS, PFDTES and PFPTES films were measured as 0.16, 0.19, 0.18, and 0.19 nm, respectively. It shows that the presence of fluorosilane films does not appear to affect the roughness values of the substrate because the films were coated as a monolayer.

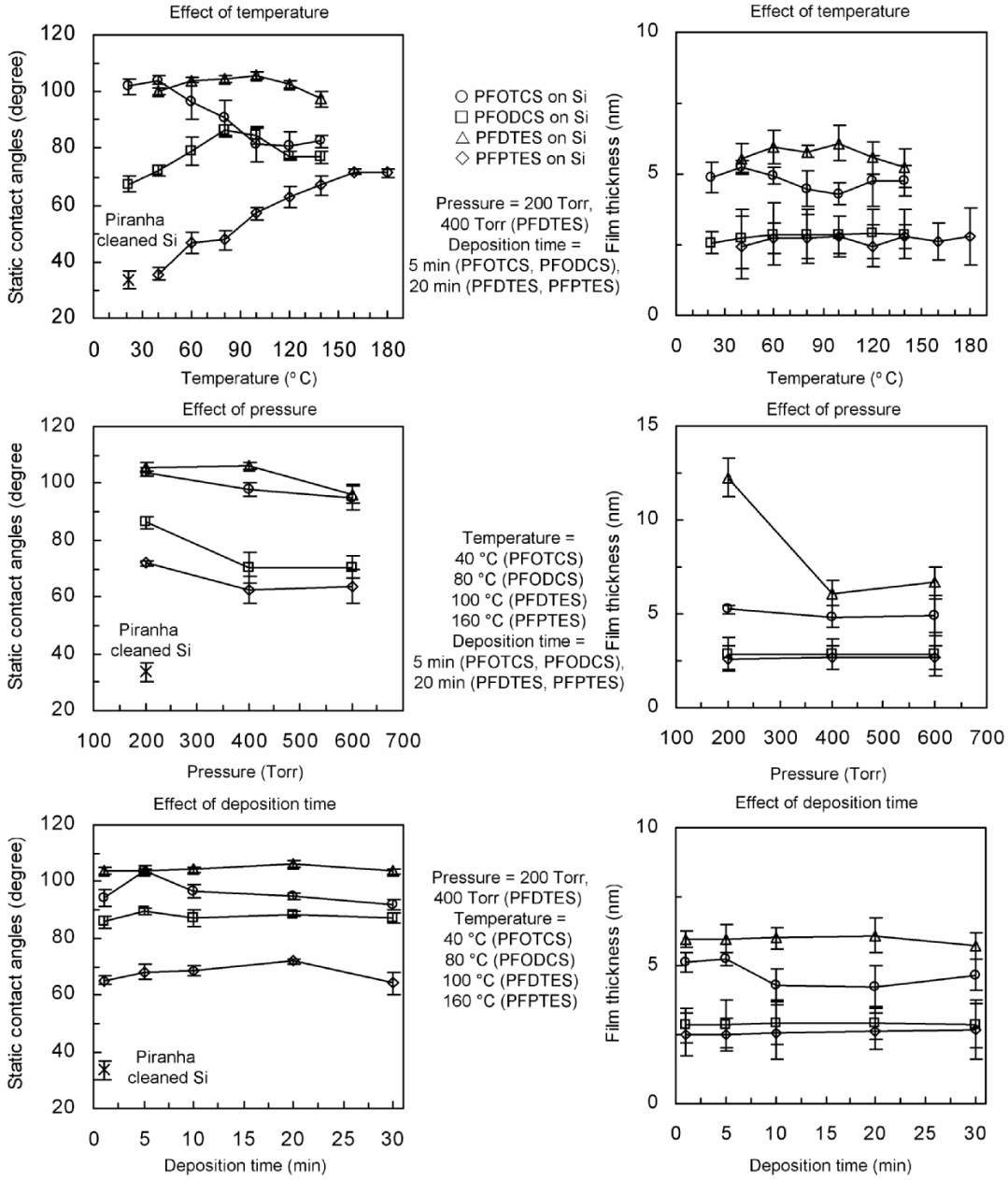

Figure 3.5: Static contact angle and film thickness measurement for optimizing the process condition as a function of temperature, pressure and deposition time.

CHAPTER 4

CONCLUSIONS

A vapor phase deposition chamber able to accommodate 100 mm silicon wafers or an array of silicon chips with microfabricated nanochannels was designed to coat uniform, conformal and ultrathin fluoropolymer and fluorosilane films on the silicon and PDMS surfaces. The deposition of these films on silicon and PDMS surfaces is important for the development of useful biomedical nanodevices. This work focuses on the development and characterization of vapor phase deposited polymer thin films on silicon and PDMS surfaces to achieve controlled surface wettability, roughness and adhesion. The deposition temperature, pressure and processing time were found to effect the surface properties of fluoropolymer and fluorosilane films. The surfaces modified by the fluoropolymer and fluorosilane films had higher water contact angles and lower adhesive forces than the wet cleaned silicon surfaces. The static contact angles of the Fluorinert^{TM} films were higher than those of CYTOP^{TM} films for all pressures, processing times and temperatures. The static contact angle value of the films on Piranha cleaned silicon was statistically identical to films on oxygen plasma treated silicon, since they have the same surface chemistry. The thicknesses of the two fluoropolymer films increased with processing time and temperature because they were deposited as multilayer films on silicon. The four fluorosilanes were deposited as monolayers, as demonstrated by thicknesses and contact angles independent of the

processing conditions. In the nanochannel system, coating on a monolayer level is required due to the nanochannel dimensions. The rms roughness values show that the presence of fluorosilane films does not affect the roughness values of the substrate, as expected for a monolayer. Reduction in coefficient of friction was found for the two fluoropolymer films as compared to the substrates. The presence of fluorosilane films reduced the adhesive force of substrates, whereas PFOTCS film has the lowest adhesive force.

REFERENCES

Auroux, P. A., Iossifidis, D., Reyes, D. R., Manz, A. (2002), "Micro Total Analysis Systems. 2. Analytical Standard Operations and Applications," *Anal. Chem.*, **74**, pp. 2637–2652.

Bhushan, B. (1999), Handbook of Micro/Nanotribology (John Wiley, New York).

Bhushan, B. and Liu, H. (2001), "Nanotribological Properties and Mechanisms of Alkylthiol and Biphenyl Thiol Self-Assembled Monolayers Studied by AFM", *Phys. Rev. B* **63,** 245412-1 to 245412-11.

Bhushan, B. (2002), Introduction to Tribology (John Wiley, New York).

Bhushan, B. (ed.) (2004), Springer Handbook of Nanotechnology (Springer-Verlag, Heidelberg, Germany).

Cox, J. D., Curry, M. S., Skirboll, S. K., Gourley, P. L., Sasaki, D. Y. (2002), "Surface passivation of a microfluidic device to glial cell adhesion: a comparison of hydrophobic and hydrophilic SAM coatings", *Biomaterials* **23**, pp. 929-935.

Desai, T. A., Hansford, D. J., Ferrari, M. (1999), "Characterization of micromachined silicon membranes for immunoisolation and bioseparation applications", *J. Membrane Sci.* **159**, pp. 221-231.

Desai, T. A., Hansford, D. J., Ferrari, M. (2000a), "Micromachined interfaces: new approaches in cell immunoisolation and biomolecular separation", *Biomol. Engr.* **17**, pp. 23-36.

Desai, T. A., Hansford, D. J., Leoni, L., Essenpreis, M., Ferrari, M. (2000b), "Nanoporous anti-fouling silicon membranes for biosensor applications", *Biosen.& Bioelect.* **15**, pp. 453-462.

Hansford, D. J., Desai, T. A., Ferrari, M., (2001), "Nano-scale Size-based Biomolecular Separation Technology," in Biochip Technology, Cheng, J.and Kricka, L. J.(Eds), pp. 341-362 (Harwood Academic Publishers, New York).

Kricka, L. J. (2001), "Microchips, Bioelectronic Chips, and Gene Chips," in Biochip Technology, Cheng, J.and Kricka, L. J.(Eds), pp. 1-16 (Harwood Academic Publishers, New York).

Lee K. K., Bhushan, B., Hansford, D. J. (2005), "Nanotribological Characterization of Fluoropolymer Thin Films for BioMEMS/NEMS Applications," *J. Vac. Sci. & Technol. A* **23(4)**, (in press).

Liu, H. and Bhushan, B. (2002), "Investigation of Nanotribological Properties of Self-Assembled Monolayers with Alkyl and Biphenyl Spacer Chains", *Ultramicroscopy* **91,** pp. 185-202.

Liu, H. and Bhushan, B. (2003a), "Adhesion and friction studies of microelectromechanical systems/nanoelectromechanical systems materials using a novel microtriboapparatus", *J. Vac. Sci. & Technol. A* **21**(4), pp. 1528-1538.

Liu, H. and Bhushan, B. (2003b), "Nanotribological Characterization of Molecularly Thick Lubricant Films for Applications to MEMS/NEMS by AFM", *Ultramicroscopy* **97,** pp. 321-340.

McDonald, J. C. and Whitesides, G. M. (2002), "Poly(dimethylsiloxane) as a Material for Fabricating Microfluidic Devices," *Acc. Chem. Res.*, **35**, pp. 491–499.

Mitchell, P. (2001), "Microfluidics-downsizing large-scale biology," *Nat. Biotech.*, **19**, pp. 717–721.

Popat, K. C., Johnson, R. W., Desai, T. A. (2002), "Characterization of vapor deposited thin silane films on silicon substrates for biomedical microdevices", *Surf. & Coat. Technol.* **154**, pp. 253-261.

Popat, K. C., Sharma, S., Johnson, R. W., Desai, T. A. (2003), "AFM analysis of organic silane thin films for bioMEMS applications", *Surf. & Interf. Analy.* **35**, pp. 205-215.

Sia S. K. and Whitesides G. M. (2003), "Microfluidic devices fabricated in poly(dimethylsiloxane) for biological studies", *Electrophoresis* **24**, pp. 3563-3576.

Wallace, R. M., Chen, P. J., Henck, S. A., Webb, D. A. (1999), "Adsorption of perfluorinated n-alkanoic acids on native aluminum oxide surfaces", *J. Vac. Sci. & Technol.A* **13** No.3, pp. 1345.

Wang, Y. and Ferrari, M. (2000), "Surface modification of micromachined silicon filters", *J. Mat. Sci.* **35**, pp. 4923-4930.

APPENDIX A

CONTACT ANGLE MEASUREMENTS

Wetting phenomena are the most often described by contact angle of a sessile or resting drop because the contact angle (θ) is a measure of wettability. Contact angle measurement is a well-known method in many fields of industry. Although contact angles are the macroscopically observable consequence of interactions at a molecular level, contact angle is a very sensitive and simple way to characterize the change of surfaces and solid/liquid interactions.

A.1 Static contact angles

Static contact angle is the angle formed at the three-phase contact of a drop of liquid with a surface when liquid is dropped onto solid surface. The static angle of a drop on solid surface is result of the balance between the cohesive forces in the liquid and the adhesive forces between the solid and the liquid. Fig. A.1 schematically illustrates sessile drops of liquids in contact with a solid surface. Young's equation (Eq. (A-1)) relates $\cos\theta$ to the local balance of forces operating at the three phase line;

$$\gamma_{lv} \cos\theta = \gamma_{sv} - \gamma_{sl} \qquad \text{(A-1)}$$

where θ = contact angle , γ = interfacial free energy, subscript : *sv* = solid-vapor, *sl* = solid-liquid, *lv* = liquid-vapor.

In practical systems, it is known that contact angles are affected by roughness and surface morphology, swelling of the solid by the contacting liquid, and heterogeneity in the chemical environment of functional groups in the interfacial region.

A.2 Dynamic contact angles

When the drop is advanced or receded on the solid surface, two different contact angles, that is, advancing angle (θa) and receding angle (θr) can be measured. These two angles commonly are called dynamic contact angle due to their dynamic nature in measurements. There are two main techniques for measuring the dynamic contact angle. These are the captive drop method and Wilhelmy plate method.

Fig. A.2 showed measurements of θa and θr by captive drop method using a sessile drop. To establish a value for θa, given small volume of liquid is gradually added to the drop, and while the needle is in the drop, the maximum contact angle is measured before the boundary of the drop has moved. For θr, on the contrary, while the needle is in the drop, a fixed volume of liquid is withdrawn, and the minimum contact angle is read before the boundary of drop has moved.

The second common method of measuring dynamic contact angle is a Wilhelmy plate technique. This is shown schematically in Fig. A.3. A rectangular sheet of the materials under test is suspended from the beam of an electrobalance with the bottom edge nearly touching the surface of liquid which is the position of zero force. The force on the plate is measured as the beaker of liquid is raised or lowered at a pre-set rate. A typical rate of immersion is 2mm/min.

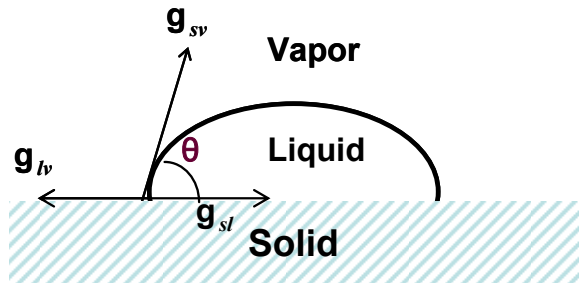

(a)

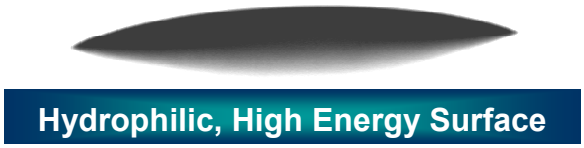

(b)

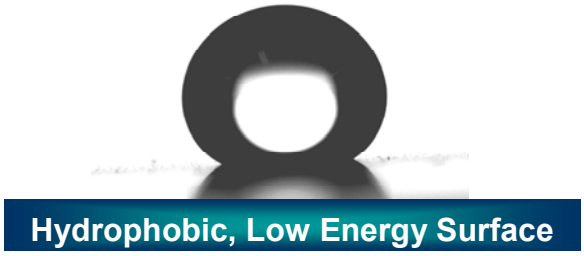

(c)

Figure A.1: (a) Balance of forces operating at triple point. Static contact angle measurements of sessile drop on (b) hydrophilic and (c) hydrophobic surfaces.

The contact angle is calculated from the measured force as shown in the Eq. (A-2).

$$F_p = p\gamma_{lv}\cos\theta\ ,\ F_b = \rho_l ghtw\ ,\ F = mg + F_p - F_b$$

$$\cos\theta = (F - mg + F_b)/(p\gamma_{lv}) \qquad \text{(A-2)}$$

where F_p = downward force of liquid on the plate, p = perimeter of the plate, γ_l = surface tension of liquid, F_b = buoyancy force, ρ_l = density of liquid, h = immersion depth, t = thickness of plate, g = acceleration due to gravity, w = width of plate, F = total force on the plate, m = mass of the plate.

The contact angle hysteresis (ΔH) can be defined as the difference between θa and θr. It is known that ΔH is a function of the surface roughness, surface polarity, chemical heterogeneity, surface penetration of the liquid molecules across the solid surface and molecular rearrangement of surface during the process of wetting and dewetting as well as the polarity of the contacting liquids. It can be also found that θa is sensitive to hydrophobic component (nonpolar portion) such as $–CF_3$ and $–CF_2$ groups and θr is sensitive to a hydrophilic component (polar portion). A decrease in the magnitude of the surface heterogeneity decreases the hysteresis.

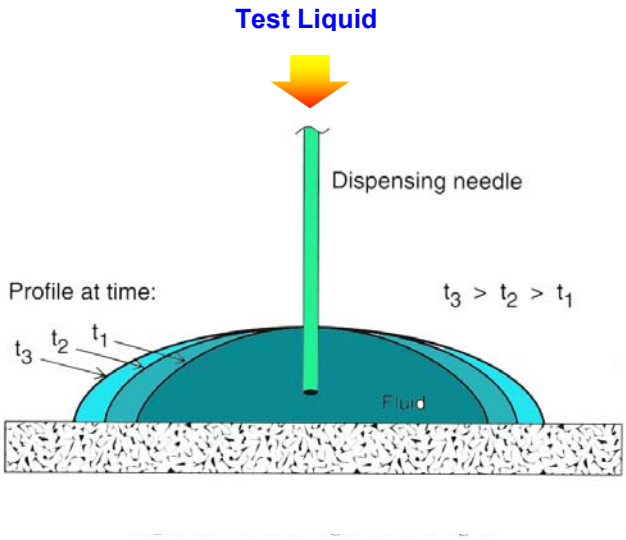

(a)

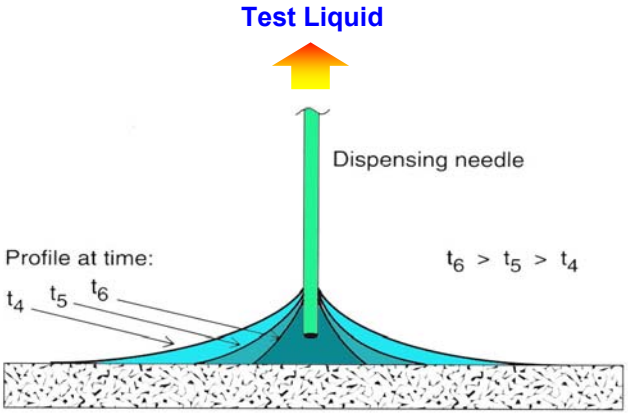

(b)

Figure A.2: Measurement of (a) the advancing and (b) receding contact angles by a captive drop method.

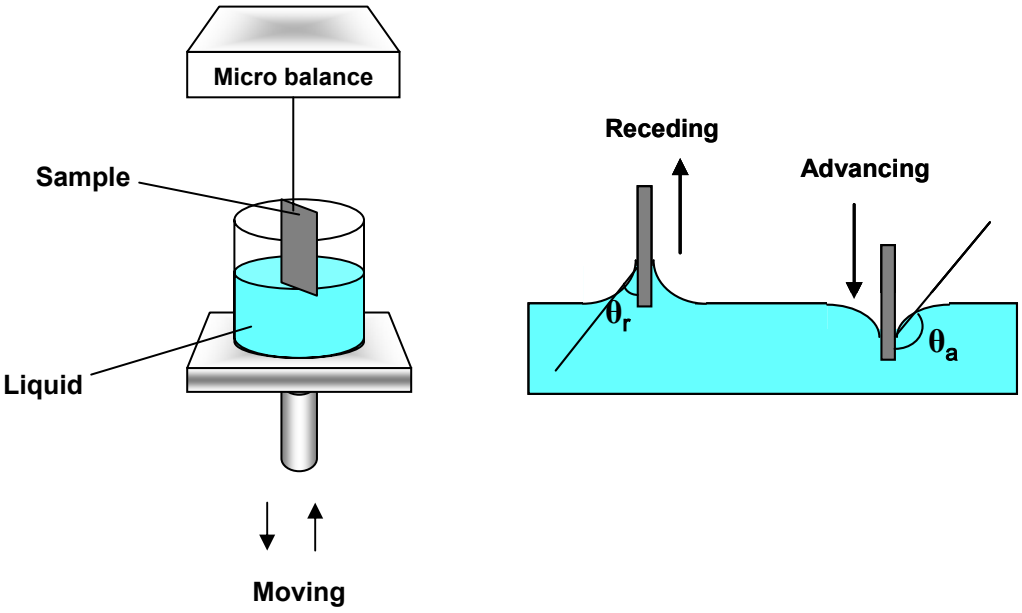

Figure A.3: Schematic diagram of the Wilhelmy plate method for measuring the advancing and receding angles.

APPENDIX B

SURFACE TREATMENTS

B.1 Wet cleaning process

One wet cleaning process for silicon wafers was in a mixture of 3:1 v/v 98% sulfuric acid and 30% hydrogen peroxide at 90 °C (known as Piranha) for 30 minutes followed by a triple rinse in deionized (DI) water. The wafers were then immersed in 49% HF solution for 10 minutes to remove the native oxide followed by another triple rinse with DI water and dried with high-pressure high-purity nitrogen gas. This is called HF cleaning.

Another surface treatment for silicon wafers was cleaning in Piranha solution (a mixture of 3:1 v/v 98% sulfuric acid: 30% hydrogen peroxide) at 90 °C for 30 minutes followed by a triple rinse in deionized water and dried with high-pressure high-purity nitrogen gas. This is called Piranha cleaning.

B.2 Oxygen plasma cleaning process

To clean the silicon wafers and the PDMS surfaces by dry method, we used an oxygen plasma cleaning system (Technics Inc., MicroRIE). In this system, optimized experimental conditions were set at O_2 flow rate of 30sccm, 187mTorr and 40 W for 10 sec, respectively. The base pressure of the system was 6-10mTorr.

Oxygen plasma treated samples were prepared using step-by-step procedures as follows:

1. Vacuum closed and vent on. Keep manual mode.
2. Open the lid, put the samples, and closes the lid.
3. Vent closed and vacuum on. Wait until the base pressure (6-10 mTorr).
4. Set the flow rate (30 sccm) and set the knob to ‘Read’ and flow the oxygen gas.
5. Turn the flow on; pressure will be up to 187 mTorr.
6. Set the power control knob to zero and power on; wait for a few minutes.
7. Turn the knob to 40 Watts and keep for 10 seconds.
8. Power off and gas flow off.
9. Vacuum closed and vent on. Wait for a few seconds to vent.
10. Open the lid, take out of the samples, and close the lid.
11. Vent closed and vacuum on.